JACS
JOURNAL OF THE AMERICAN CHEMICAL SOCIETY
pubs.acs.org/JACS
Communication

Multiplexed Single-Molecule Experiments Reveal Nucleosome Invasion Dynamics of the Cas9 Genome Editor

Kristina Makasheva, Louise C. Bryan, Carolin Anders, Sherin Panikulam, Martin Jinek, and Beat Fierz*

Cite This: J. Am. Chem. Soc. 2021, 143, 16313−16319

ABSTRACT: Single-molecule measurements provide detailed mechanistic insights into molecular processes, for example in genome regulation where DNA access is controlled by nucleosomes and the chromatin machinery. However, real-time single-molecule observations of nuclear factors acting on defined chromatin substrates are challenging to perform quantitatively and reproducibly. Here we present XSCAN (multiplexed single-molecule detection of chromatin association), a method to parallelize single-molecule experiments by simultaneous imaging of a nucleosome library, where each nucleosome type carries an identifiable DNA sequence within its nucleosomal DNA. Parallel experiments are subsequently spatially decoded, via the detection of specific binding of dye-labeled DNA probes. We use this method to reveal how the Cas9 nuclease overcomes the nucleosome barrier when invading chromatinized DNA as a function of PAM position.

Chromatin, which organizes eukaryotic DNA, is a dynamic structure,[1] and its dynamic modes are critical for genome regulation. Transient DNA unwrapping from the nucleosome core enables transcription factor binding,[2] nucleosomes are mobilized by remodeling factors,[3] RNA polymerase,[4] or repair enzymes,[5] and chromatin structure is constantly reshaped by interacting proteins.[6,7] The underlying molecular mechanisms involve interactions between nuclear factors and chromatin, modulated by DNA sequence or histone post-translational modifications (PTMs), over multiple spatial and temporal scales. Real-time single-molecule imaging, by not being limited by ensemble averaging, provides a unique window into such multiscale processes on a mechanistic level.

The clustered regularly interspaced short palindromic repeats (CRISPR)-associated 9 (Cas9) nuclease is an important tool for genome editing.[8,9] Its specificity is programmed via a single guide RNA (sgRNA).[8] Complementary DNA motifs, flanked by a protospacer adjacent motif (PAM), are bound by Cas9, and a RNA-DNA hybrid R-loop is formed, followed by DNA cleavage.[10] This enables genome editing with single-nucleotide accuracy.[8,9] Conversely, catalytically inactive Cas9[11] (dCas9) can be employed to recruit enzymatic activities to specific genomic loci for epigenome editing.[12] It is thus important to understand how Cas9 interacts with chromatin. Single-molecule studies showed that Cas9 can undergo localized sliding in the search for PAM sites.[13,14] PAM recognition is followed by localized DNA unwinding and directional R-loop formation, resulting in a long-lived complex.[14−17] Enzymatic studies revealed that Cas9 (and the related Cas12a) nuclease activity is reduced by nucleosomes.[18−21] To investigate if this activity loss originates from impaired DNA access or from reduced residence time and inefficient catalysis, we aimed to systematically image chromatin invasion by Cas9 in real-time.

We previously employed single-molecule total internal reflection fluorescence (sm-TIRF) microscopy to measure interaction kinetics between chemically defined oligo- or mononucleosomes (MN) and nuclear proteins.[22] Fluorescently labeled chromatin constructs are immobilized in a flow cell. Subsequently, chromatin binding factors, carrying a fluorescent dye of a different spectral range, are injected and binding interactions are detected by fluorescence colocalization. However, this technique is limited to a single chromatin type per experiment, and does not allow for direct comparison or competition between different chromatin constructs. This is a particular issue for the determination of binding kinetics, which are highly sensitive to concentration variations between measurements. Methods have been put forward to perform binding experiments in parallel, including spatially separating substrates,[23] employing multichannel microfluidic cells,[24] or combining sm-TIRF with *in situ* single-molecule DNA sequencing.[25] However, both the complexity of existing methods and their limitations in the number of binding substrates and applicable experimental conditions prompted us to develop a novel approach.

Here we introduce XSCAN, a robust and expandable parallelized single-molecule method to simultaneously observe nuclear factors acting on multiple chromatin types in a single experiment (Figure 1). We then apply XSCAN to systematically map the nucleosome impact on Cas9 binding kinetics.

We envisaged using a DNA-barcoding strategy to parallelize single-molecule experiments on chromatin. Mono- or oligonucleosomes (containing different DNA sequences, histone variants, or PTM patterns) are assembled using DNA that

Received: June 17, 2021
Published: October 1, 2021

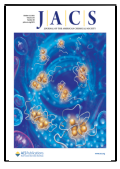

https://doi.org/10.1021/jacs.1c06195
J. Am. Chem. Soc. 2021, 143, 16313−16319

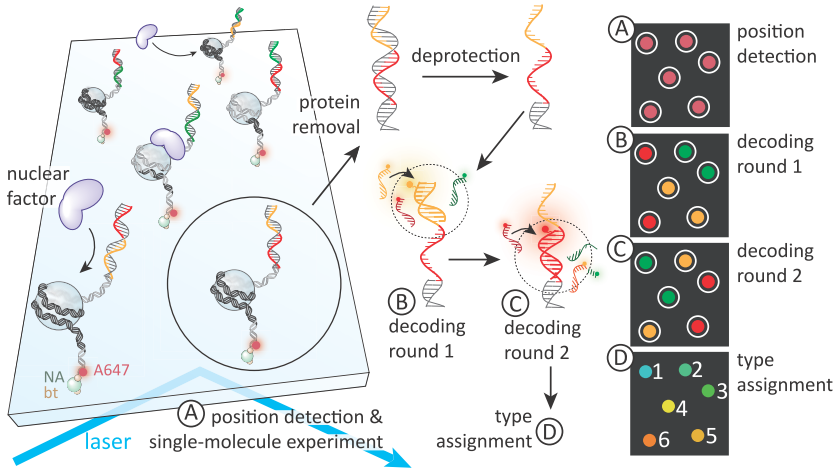

Figure 1. General scheme of the XSCAN approach.

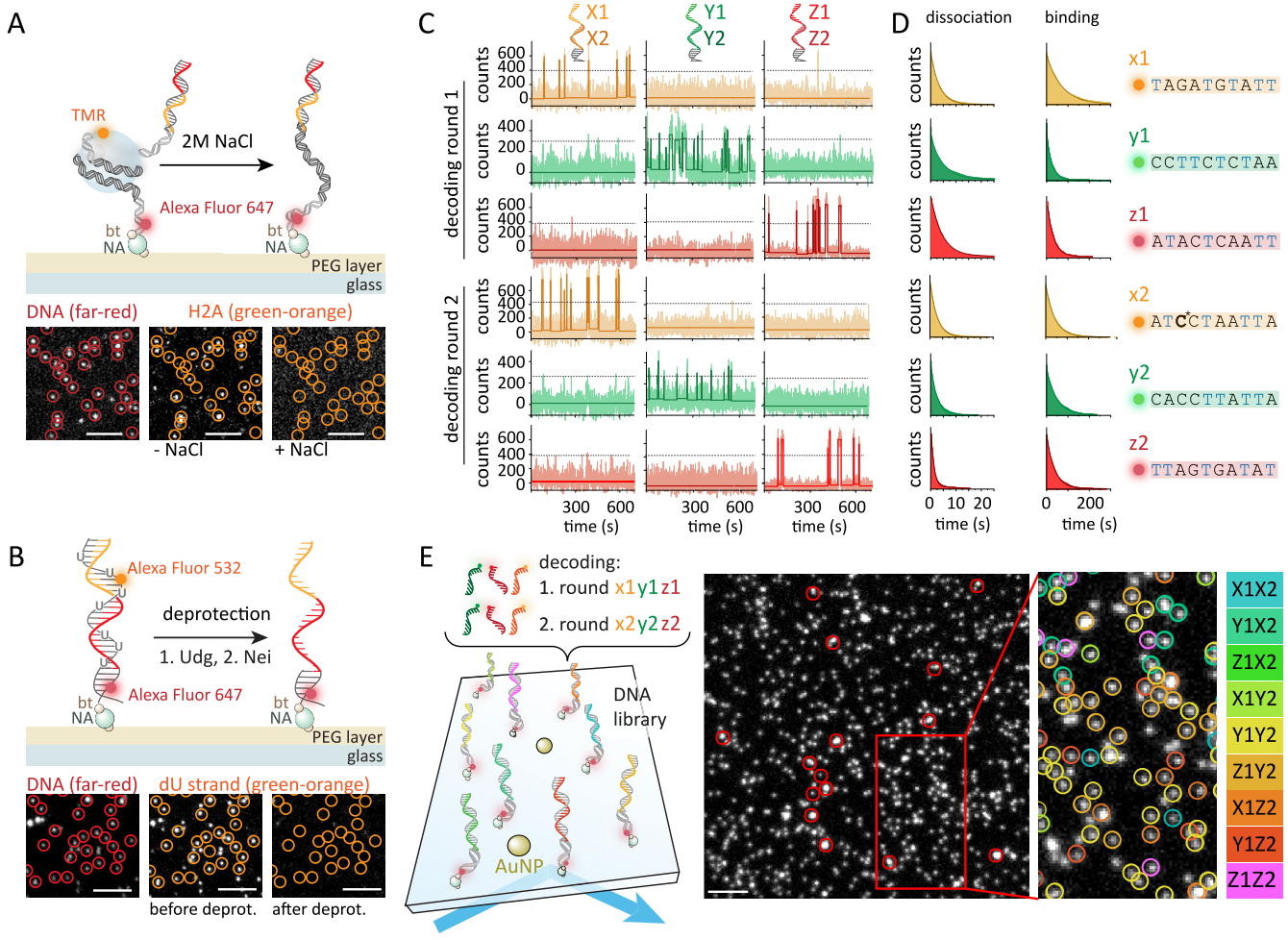

Figure 2. (A) Protein removal by high-salt wash: sm-TIRF images of nucleosome positions (left) and histone presence before (middle) and after wash (right). bt-NA: biotin-neutravidin. (B) Barcode deprotection: sm-TIRF images of DNA positions (left) and barcodes before (middle) and after deprotection (right). (C) Fluorescent time traces showing binding events for indicated DNA barcodes/decoding rounds. (D) Decoder sequences and cumulative histograms of dissociation and binding times fitted with monoexponential functions. Fit results: Table S1. (E) Left: Scheme of a decoding experiment, AuNP: gold nanoparticles. Middle: sm-TIRF image showing DNA locations before decoding (AuNP: red circles). Right: color-coded identified barcodes. All scale bars: 5 μm.

contains sequence barcodes indicating the chromatin type.[26,27] Barcoded nucleosomes are randomly immobilized in a flow cell and used in single-molecule experiments, including, but not limited to, dynamic interaction studies (Figure 1A). For identification of the nucleosome type at each position, all proteins are removed. Subsequently, the remaining DNA is

https://doi.org/10.1021/jacs.1c06195
J. Am. Chem. Soc. 2021, 143, 16313−16319

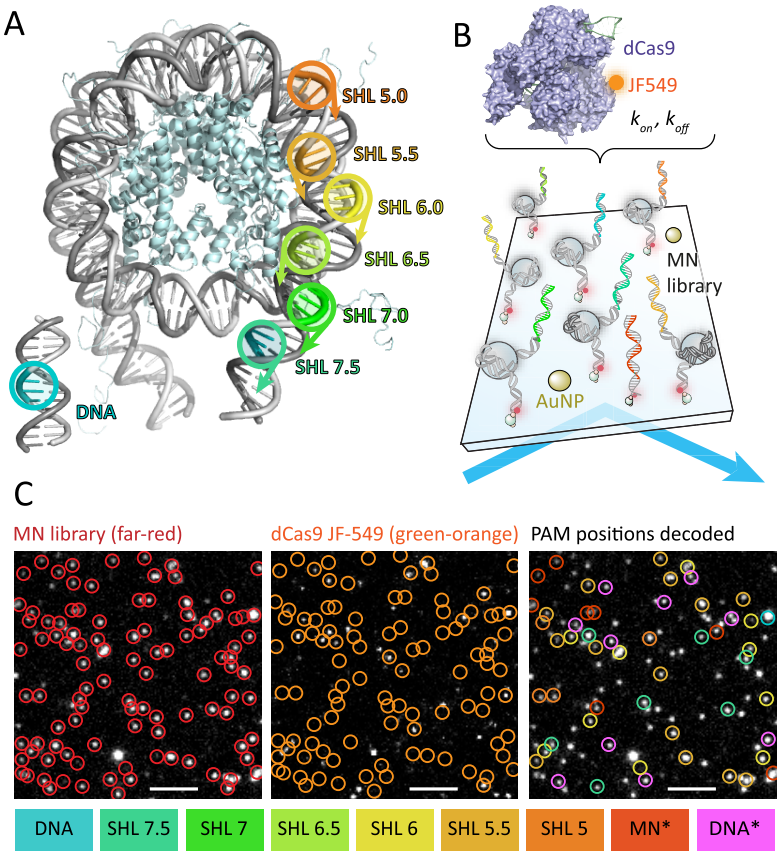

Figure 3. (A) Nucleosome structure (PDB: 1KX5)[34] with PAM positions. Arrows indicate target sequence orientation. (B) Scheme of XSCAN assay to measure dCas9 binding kinetics. (C) sm-TIRF images showing nucleosomes positions (left), dCas9 binding (middle), and identified nucleosomes positions (right, color-coded; DNA: naked DNA, MN*/DNA*: nucleosome/DNA without target). Scale bars: 5 μm.

spatially decoded to reveal the nucleosome identity. We identified two critical requirements for this decoding approach. The method should (1) be compatible with single-molecule experiments, e.g. allow polyethylene glycol surface passivation,[28] and (2) should be fast and yield a high identification success rate. This is necessary to obtain reliable single-molecule statistics.

After evaluating different approaches we settled on a decoding strategy based on detecting binding of fluorescent 10-mer oligonucleotides ("decoder" probes) to the chromatin-associated barcode sequences[29,30] (Figure 1B). A barcode design, based on several adjacent binding sites, enabled performing multiple "rounds" of decoding (Figure 1C). Thus, we could maximize the number of barcodes identified with a limited number of spectrally separated fluorescent dyes. Finally, from the combination of fluorescence detections, the barcode, and thus chromatin type, could be assigned (Figure 1D).

To develop XSCAN, we had to establish key procedures. As decoding works best on naked DNA, we first tested full protein removal in the flow chamber, while retaining the immobilized DNA. Using nucleosomes containing tetramethylrhodamine (TMR)-labeled H2A (Figure S1), all histones were removed with a 2.5 M NaCl wash (Figure 2A). Second, we considered that the single-stranded DNA (ssDNA) barcodes could interfere with preceding single-molecule binding assays. We thus embedded the barcode sequences in double-stranded DNA (dsDNA), only to be deprotected directly before decoding. Deprotection is achieved by incorporating deoxyuridines (dU) into the barcode-complementary DNA strands, allowing their selective degradation by Uracil DNA Glycosylase (Udg) followed by Endonuclease VIII (Nei).[31,32] We monitored barcode liberation via fluorescence, revealing a 95% deprotection efficiency (Figure 2B). Third, we designed barcode/decoder sequences. We prepared three pairs of decoders, x1, x2, y1, y2, and z1, z2, where the number designates the decoding round, and the letter indicates the dye: Alexa Fluor 532 (x), Alexa Fluor 488 (y), and Alexa Fluor 647 (z). The decoder sequences were based on DNA-PAINT imager strands.[30] They were further modified to contain at least 2−3 equally spaced dTs for deprotection, and any sequence homology was minimized (<3bp) to ensure specificity (Figure 2C, D, Table S1). In parallel, we produced fluorescently labeled DNA templates for nucleosome assembly, derived from the 601 Widom nucleosome positioning sequence,[33] and bearing each one of the nine possible barcodes (designated by capital letters, see Figure S1, Tables S2, S3).

With this set of decoders and barcoded templates, we assessed decoder specificity and binding kinetics. Initially, we used three DNA templates with barcodes X1X2, Y1Y2, and Z1Z2 (Figure 2C), which were randomly immobilized, and their locations were determined in the far-red channel, after which all dyes were bleached and barcodes were liberated. Gold nanoparticles allowed image alignment across the whole experiments. A first round of 3-color colocalization imaging of a mixture of 10 nM of each x1, y1, and z1 decoders, followed by a second round of decoding using x2, y2, and z2 decoders,

https://doi.org/10.1021/jacs.1c06195
J. Am. Chem. Soc. 2021, 143, 16313−16319

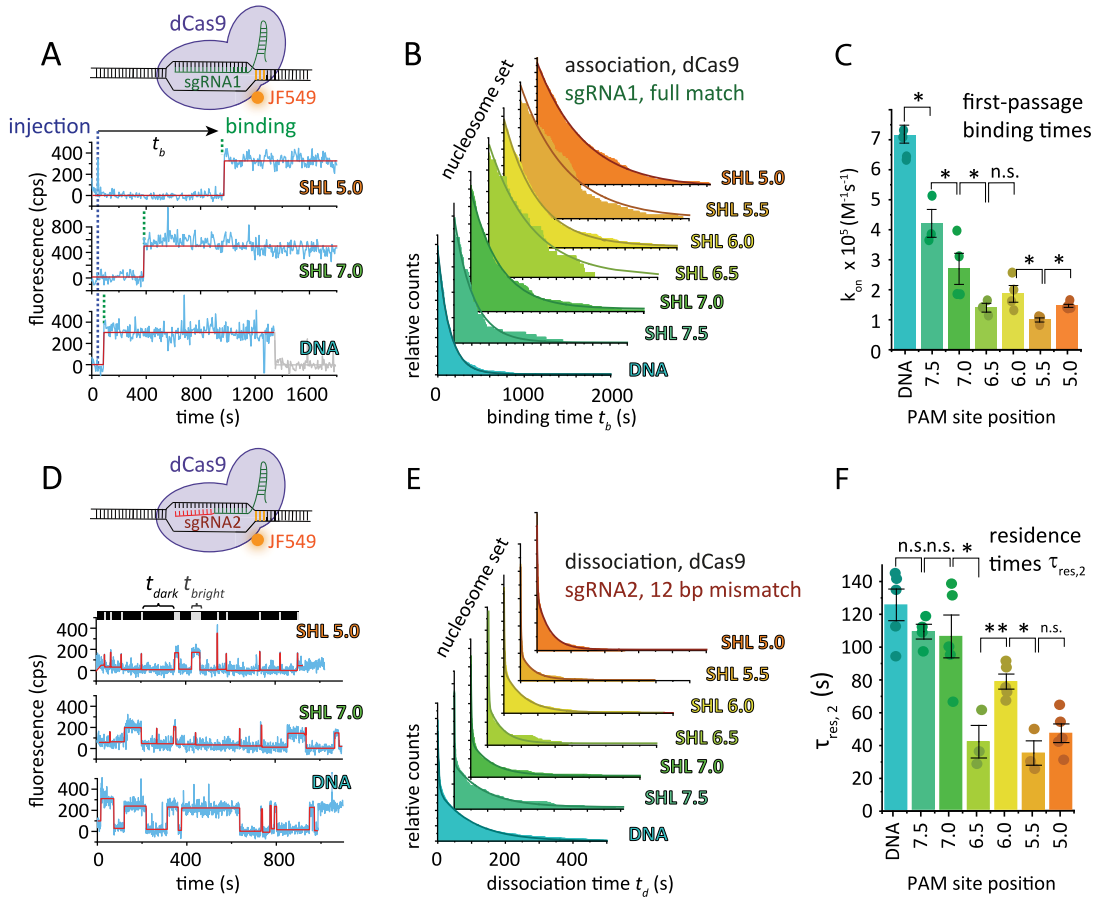

Figure 4. (A) Fluorescence time traces of dCas9 binding to indicated nucleosomes/DNA, fitted by a step algorithm (red). (B) Cumulative histograms of dCas binding times (t_b), fitted by monoexponential function. For results, see (C), Figure S5 and Table S5. (C) Association rates for dCas9/sgRNA1 binding. (D) Fluorescence time traces of dCas9/sgRNA2 to indicated nucleosomes/DNA, fitted by a step algorithm (red). (E) Cumulative histograms of dCas/sgRNA2 dissociation times (t_d), fitted by biexponential function. For all results, see (F), Figure S6 and Table S6. (F) Specific dissociation time constants $\tau_{res,2}$ for dCas9/sgRNA2 binding. Error bars: SD, n = 3−5, two-tailed Student's t test *: p = 0.01−0.05, **: p = 0.001−0.01, n.s.: not significant.

revealed specific barcode recognition, decoder residence times of 1.6−4.6 s, and binding rate constants (k_{on}) of (0.6−2.4) × 10^6 M^{-1} s^{-1} (Figure 2D, Table S1). We then proceeded to decode a full set of 9 barcoded DNA templates (Figure 2E), and the immobilized DNA templates were identified with a success rate of 65% (Figure 2E). False positive detections, i.e. one barcode bound by several decoders in the same round (below 0.5%), or lack of decoder binding in any round, resulted in the exclusion of the position from analysis. We were usually able to assign ∼1000 immobilized molecules to 1 of 9 DNA types in a single field-of-view. Together, these findings show that XSCAN can be used to multiplex single-molecule experiments.

Having a functional methodology at hand, we proceeded to investigate the chromatin invasion dynamics of Cas9 using XSCAN. We reconstituted a barcoded set of nucleosomes containing a target sequence including a PAM, placed at increasingly internal positions within the nucleosome. Positions were designated by the superhelix location (SHL)[35] of the PAM, between 7.5 and 5.0 (Figure 3A, Tables S2, 3). The final set, which further included naked DNA with a target sequence as well as both naked DNA and nucleosomes without a target, was stochastically immobilized in the flow chamber, and positions were determined. For all binding experiments we used catalytically inactive dCas9 protein, labeled with the dye JF-549[36] via a peptide tag[37] and containing the appropriate sgRNA (Figure S2, Table S4). In a typical experiment, we imaged at a 0.2−10 Hz frame rate and directly monitored the injection of dCas9 at a concentration of 8−16 nM, chosen such that individual, nonoverlapping binding events could be detected as fluorescent spots in the green-orange channel (Figure 3B, C). After ∼2500 s, all remaining dyes were bleached, the channel was washed, barcodes were enzymatically deprotected, and two rounds of decoding were performed, to identify the DNA/nucleosomes types at each position (Figure 3C).

In a first set of measurements, we determined the time required for dCas9, containing an sgRNA fully complementary to the 20 bp target sequence (sgRNA1, Table S4), to invade the nucleosome structure at different SHL (Figure 4A). Injected dCas9 explored DNA and nucleosomes via transient (1−10 s) nonspecific binding events (Figure S3). As soon as dCas9 found its target site, it formed a long-lived complex that did not dissociate within the time frame of the experiment (Figure S4). In the competitive XSCAN experiment, dCas9 first bound to naked DNA (Figure 4B, C, Table S5), following exponential kinetics with k_{on} = (6.89 ± 1.04) × 10^5 M^{-1} s^{-1}. Next, outer nucleosomal positions (SHL 7.5 and 7.0) were bound, whereas dCas9 invasion at more internal positions (SHL 6.5−5.0) occurred with a 5-fold reduction in k_{on},

https://doi.org/10.1021/jacs.1c06195
J. Am. Chem. Soc. 2021, 143, 16313−16319

compared to naked DNA. This indicates that nucleosome invasion is coupled to transient DNA unwrapping events at the nucleosome periphery.[38] Moreover, dCas9 showed sensitivity for the rotational orientation of the PAM site, as binding to SHL 6.5 and 5.5 (where PAM is facing toward the histone core) was slower (Figure 4C). Finally, for a fraction of nucleosomes, in particular for internal and inward-facing PAM positions, no binding was observed (Figure S5), suggesting that the complete kinetic process is not captured in these cases on the achievable experimental time scale. Together, the reduction in first-passage DNA binding in nucleosomes is a likely reason for the impairment of Cas9 nuclease activity in nucleosomes[18−21] (Figure S6). Additional effects, such as inhibition of full R-loop formation, may however further contribute.

Our data show that the residence time of dCas9, when bound to DNA and forming a full 20 bp RNA-DNA hybrid, is on the time scale of hours, even within a nucleosome. However, mismatches between sgRNA and the DNA target sequences alter the Cas9 DNA binding process[39] and can result in a strong increase in the dissociation rate on naked DNA.[15] Moreover, the nucleosome structure has been observed to suppress off-target DNA cleavage.[40] We thus decided to employ XSCAN to profile the nucleosome binding kinetics of dCas9 containing an sgRNA with 12 PAM-distal mismatches (sgRNA2, Table S4). Imaging at 1 Hz, we observed a subpopulation of short binding events that lasted 1−4 s ($\tau_{res,1}$) and which were not significantly different across DNA and nucleosome types (Figures 4D, E, S7). As they also occurred in dCas9 lacking an sgRNA (Figure S3), they likely reflect nonspecific DNA binding. A second population of events, which we attributed to specific binding of dCas9/sgRNA2 to the target sequence, lasted tens to hundreds of seconds and were encountered at a higher frequency at peripheral positions (Figure 4E, F). For naked DNA, we observed $\tau_{res,2}$ = 121 ± 21 s, whereas residence times were reduced by up to 3-fold at nucleosome internal sites. Interestingly, we again observed a pattern of inward facing PAM yielding shorter residence times (Figure 4E). Finally, k_{on} also progressively decreased for increasingly internal positions, similar to experiments with sgRNA1 (Figure S7). These results reveal that nucleosomes alter the free energy profile of dCas9 chromatin access, as binding is impaired and dissociation is accelerated at internal sites. Moreover, access to PAM sites facing toward the histone core carries a free energy penalty of around kT, demonstrating that rotational orientation of the DNA plays an additional role.

In conclusion, we have established XSCAN as a method to multiplex single-molecule chromatin experiments. In its current implementation, XSCAN allows us to simultaneously perform single-molecule experiments using up to nine different chromatin constructs simultaneously and in direct competition, in a single microfluidic flow cell. The method is specific, versatile, and expandable to 27 or 81 templates by adding a third or fourth decoding round. Moreover, the procedure is rapid (~20 min/round) and can be automated using microfluidics. We thus believe that this represents an effective approach for the exploration of the dynamic chromatin landscape and beyond. Here, we used XSCAN to observe the invasion process of dCas9 into nucleosomal DNA. We conclude that nucleosomes hinder the initial PAM-dependent target recognition by dCas9 through a combination of several effects (see also Supporting Information). First, target binding is coupled to local DNA unwrapping, in agreement with observations for other nucleosome binding factors.[2,38] The PAM position on the nucleosome surface has an additional effect, indicating that dCas9 initially engages the nucleosome in a wrapped state.[41] Finally, nucleosomes shorten dCas9 off-target binding, potentially via dynamic competition with histone proteins within the nucleosomes,[42] consistent with prior observations that nucleosomes repress off-target DNA cleavage *in vitro*.[40] Thus, chromatin might increase the specificity of Cas9 genome editing *in vivo* by providing a kinetic barrier to off-target binding and cleavage. Our results shed light onto the mechanism of nucleosome inhibition of Cas9 nuclease activity which is critical to the success of genome targeting or epigenome editing applications.

■ ASSOCIATED CONTENT

Supporting Information

The Supporting Information is available free of charge at https://pubs.acs.org/doi/10.1021/jacs.1c06195.

Synthetic and analysis methods, analytical characterization of all purified reagents, Figures S1−S7 and Tables S1−S6 (PDF)

■ AUTHOR INFORMATION

Corresponding Author

Beat Fierz − *Laboratory of Biophysical Chemistry of Macromolecules, Institute of Chemical Sciences and Engineering (ISIC), École Polytechnique Fédérale de Lausanne (EPFL), 1015 Lausanne, Switzerland;* orcid.org/0000-0002-2991-3044; Email: beat.fierz@epfl.ch

Authors

Kristina Makasheva − *Laboratory of Biophysical Chemistry of Macromolecules, Institute of Chemical Sciences and Engineering (ISIC), École Polytechnique Fédérale de Lausanne (EPFL), 1015 Lausanne, Switzerland;* orcid.org/0000-0002-0645-6848

Louise C. Bryan − *Laboratory of Biophysical Chemistry of Macromolecules, Institute of Chemical Sciences and Engineering (ISIC), École Polytechnique Fédérale de Lausanne (EPFL), 1015 Lausanne, Switzerland*

Carolin Anders − *Department of Biochemistry, University of Zurich, 8057 Zurich, Switzerland*

Sherin Panikulam − *Department of Biochemistry, University of Zurich, 8057 Zurich, Switzerland*

Martin Jinek − *Department of Biochemistry, University of Zurich, 8057 Zurich, Switzerland*

Complete contact information is available at: https://pubs.acs.org/10.1021/jacs.1c06195

Notes

The authors declare no competing financial interest.

■ ACKNOWLEDGMENTS

B.F. is supported by the European Research Council (ERC) (ERC-CoG-724022), the Swiss National Science Foundation (SNSF) (31003A_173169), and Ecole Polytechnique Fédérale de Lausanne (EPFL). M.J. is supported by the SNSF (31003A_182567) and ERC (ERC-CoG-820152). M.J. is an International Research Scholar of the Howard Hughes Medical Institute, and Vallee Scholar of the Bert L & N Kuggie Vallee

Foundation. We thank Alexandra Teslenko, Maxime Mivelaz, and Ruud Hovius for comments on the manuscript.

REFERENCES

(1) Bell, O.; Tiwari, V. K.; Thoma, N. H.; Schubeler, D. Determinants and dynamics of genome accessibility. *Nat. Rev. Genet.* **2011**, *12* (8), 554−564.
(2) Li, G.; Widom, J. Nucleosomes facilitate their own invasion. *Nat. Struct. Mol. Biol.* **2004**, *11* (8), 763−9.
(3) Clapier, C. R.; Cairns, B. R. The Biology of Chromatin Remodeling Complexes. *Annu. Rev. Biochem.* **2009**, *78*, 273−304.
(4) Kobayashi, W.; Kurumizaka, H. Structural transition of the nucleosome during chromatin remodeling and transcription. *Curr. Opin. Struct. Biol.* **2019**, *59*, 107−114.
(5) Matsumoto, S.; Cavadini, S.; Bunker, R. D.; Grand, R. S.; Potenza, A.; Rabl, J.; Yamamoto, J.; Schenk, A. D.; Schubeler, D.; Iwai, S.; Sugasawa, K.; Kurumizaka, H.; Thoma, N. H. DNA damage detection in nucleosomes involves DNA register shifting. *Nature* **2019**, *571* (7763), 79−84.
(6) Li, W.; Chen, P.; Yu, J.; Dong, L.; Liang, D.; Feng, J.; Yan, J.; Wang, P. Y.; Li, Q.; Zhang, Z.; Li, M.; Li, G. FACT Remodels the Tetranucleosomal Unit of Chromatin Fibers for Gene Transcription. *Mol. Cell* **2016**, *64* (1), 120−133.
(7) Kilic, S.; Felekyan, S.; Doroshenko, O.; Boichenko, I.; Dimura, M.; Vardanyan, H.; Bryan, L. C.; Arya, G.; Seidel, C. A. M.; Fierz, B. Single-molecule FRET reveals multiscale chromatin dynamics modulated by HP1alpha. *Nat. Commun.* **2018**, *9* (1), 235.
(8) Jinek, M.; Chylinski, K.; Fonfara, I.; Hauer, M.; Doudna, J. A.; Charpentier, E. A programmable dual-RNA-guided DNA endonuclease in adaptive bacterial immunity. *Science* **2012**, *337* (6096), 816−21.
(9) Doudna, J. A.; Charpentier, E. Genome editing. The new frontier of genome engineering with CRISPR-Cas9. *Science* **2014**, *346* (6213), 1258096.
(10) Jiang, F.; Taylor, D. W.; Chen, J. S.; Kornfeld, J. E.; Zhou, K.; Thompson, A. J.; Nogales, E.; Doudna, J. A. Structures of a CRISPR-Cas9 R-loop complex primed for DNA cleavage. *Science* **2016**, *351* (6275), 867−71.
(11) Qi, L. S.; Larson, M. H.; Gilbert, L. A.; Doudna, J. A.; Weissman, J. S.; Arkin, A. P.; Lim, W. A. Repurposing CRISPR as an RNA-guided platform for sequence-specific control of gene expression. *Cell* **2013**, *152* (5), 1173−83.
(12) Nakamura, M.; Gao, Y.; Dominguez, A. A.; Qi, L. S. CRISPR technologies for precise epigenome editing. *Nat. Cell Biol.* **2021**, *23* (1), 11−22.
(13) Globyte, V.; Lee, S. H.; Bae, T.; Kim, J. S.; Joo, C., CRISPR/Cas9 searches for a protospacer adjacent motif by lateral diffusion. *EMBO J.* **2019**, *38* (4). DOI: 10.15252/embj.201899466.
(14) Sternberg, S. H.; Redding, S.; Jinek, M.; Greene, E. C.; Doudna, J. A. DNA interrogation by the CRISPR RNA-guided endonuclease Cas9. *Nature* **2014**, *507* (7490), 62−7.
(15) Singh, D.; Sternberg, S. H.; Fei, J.; Doudna, J. A.; Ha, T. Real-time observation of DNA recognition and rejection by the RNA-guided endonuclease Cas9. *Nat. Commun.* **2016**, *7*, 12778.
(16) Knight, S. C.; Xie, L.; Deng, W.; Guglielmi, B.; Witkowsky, L. B.; Bosanac, L.; Zhang, E. T.; El Beheiry, M.; Masson, J. B.; Dahan, M.; Liu, Z.; Doudna, J. A.; Tjian, R. Dynamics of CRISPR-Cas9 genome interrogation in living cells. *Science* **2015**, *350* (6262), 823−6.
(17) Dagdas, Y. S.; Chen, J. S.; Sternberg, S. H.; Doudna, J. A.; Yildiz, A. A conformational checkpoint between DNA binding and cleavage by CRISPR-Cas9. *Science advances* **2017**, *3* (8), No. eaao0027.
(18) Hinz, J. M.; Laughery, M. F.; Wyrick, J. J. Nucleosomes Inhibit Cas9 Endonuclease Activity in Vitro. *Biochemistry* **2015**, *54* (48), 7063−6.
(19) Horlbeck, M. A.; Witkowsky, L. B.; Guglielmi, B.; Replogle, J. M.; Gilbert, L. A.; Villalta, J. E.; Torigoe, S. E.; Tjian, R.; Weissman, J. S., Nucleosomes impede Cas9 access to DNA in vivo and in vitro. *eLife* **2016**, *5*. DOI: 10.7554/eLife.12677.
(20) Isaac, R. S.; Jiang, F.; Doudna, J. A.; Lim, W. A.; Narlikar, G. J.; Almeida, R., Nucleosome breathing and remodeling constrain CRISPR-Cas9 function. *eLife* **2016**, *5*. DOI: 10.7554/eLife.13450.
(21) Strohkendl, I.; Saifuddin, F. A.; Gibson, B. A.; Rosen, M. K.; Russell, R.; Finkelstein, I. J., Inhibition of CRISPR-Cas12a DNA targeting by nucleosomes and chromatin. *Science advances* **2021**, *7* (11). DOI: 10.1126/sciadv.abd6030.
(22) Kilic, S.; Bachmann, A. L.; Bryan, L. C.; Fierz, B. Multivalency governs HP1alpha association dynamics with the silent chromatin state. *Nat. Commun.* **2015**, *6*, 7313.
(23) Wang, Y.; Guo, L.; Golding, I.; Cox, E. C.; Ong, N. P. Quantitative transcription factor binding kinetics at the single-molecule level. *Biophys. J.* **2009**, *96* (2), 609−20.
(24) Khamis, H.; Rudnizky, S.; Melamed, P.; Kaplan, A., Single molecule characterization of the binding kinetics of a transcription factor and its modulation by DNA sequence and methylation. *bioRxiv Preprint* **2021**, (May 20, 2021), DOI: 10.1101/2021.05.19.444789 (accessed 2021-09-21).
(25) Shema, E.; Jones, D.; Shoresh, N.; Donohue, L.; Ram, O.; Bernstein, B. E. Single-molecule decoding of combinatorially modified nucleosomes. *Science* **2016**, *352* (6286), 717−21.
(26) Nguyen, U. T.; Bittova, L.; Muller, M. M.; Fierz, B.; David, Y.; Houck-Loomis, B.; Feng, V.; Dann, G. P.; Muir, T. W. Accelerated chromatin biochemistry using DNA-barcoded nucleosome libraries. *Nat. Methods* **2014**, *11* (8), 834−40.
(27) Dann, G. P.; Liszczak, G. P.; Bagert, J. D.; Muller, M. M.; Nguyen, U. T. T.; Wojcik, F.; Brown, Z. Z.; Bos, J.; Panchenko, T.; Pihl, R.; Pollock, S. B.; Diehl, K. L.; Allis, C. D.; Muir, T. W. ISWI chromatin remodellers sense nucleosome modifications to determine substrate preference. *Nature* **2017**, *548* (7669), 607−611.
(28) Roy, R.; Hohng, S.; Ha, T. A practical guide to single-molecule FRET. *Nat. Methods* **2008**, *5* (6), 507−16.
(29) Jungmann, R.; Steinhauer, C.; Scheible, M.; Kuzyk, A.; Tinnefeld, P.; Simmel, F. C. Single-molecule kinetics and super-resolution microscopy by fluorescence imaging of transient binding on DNA origami. *Nano Lett.* **2010**, *10* (11), 4756−61.
(30) Jungmann, R.; Avendano, M. S.; Woehrstein, J. B.; Dai, M.; Shih, W. M.; Yin, P. Multiplexed 3D cellular super-resolution imaging with DNA-PAINT and Exchange-PAINT. *Nat. Methods* **2014**, *11* (3), 313−8.
(31) Bitinaite, J.; Rubino, M.; Varma, K. H.; Schildkraut, I.; Vaisvila, R.; Vaiskunaite, R. USER friendly DNA engineering and cloning method by uracil excision. *Nucleic Acids Res.* **2007**, *35* (6), 1992−2002.
(32) Stivers, J. T.; Jiang, Y. L. A mechanistic perspective on the chemistry of DNA repair glycosylases. *Chem. Rev.* **2003**, *103* (7), 2729−59.
(33) Lowary, P. T.; Widom, J. New DNA sequence rules for high affinity binding to histone octamer and sequence-directed nucleosome positioning. *J. Mol. Biol.* **1998**, *276* (1), 19−42.
(34) Davey, C. A.; Sargent, D. F.; Luger, K.; Maeder, A. W.; Richmond, T. J. Solvent mediated interactions in the structure of the nucleosome core particle at 1.9 a resolution. *J. Mol. Biol.* **2002**, *319* (5), 1097−113.
(35) Luger, K.; Mader, A. W.; Richmond, R. K.; Sargent, D. F.; Richmond, T. J. Crystal structure of the nucleosome core particle at 2.8 A resolution. *Nature* **1997**, *389* (6648), 251−60.
(36) Grimm, J. B.; English, B. P.; Chen, J.; Slaughter, J. P.; Zhang, Z.; Revyakin, A.; Patel, R.; Macklin, J. J.; Normanno, D.; Singer, R. H.; Lionnet, T.; Lavis, L. D. A general method to improve fluorophores for live-cell and single-molecule microscopy. *Nat. Methods* **2015**, *12* (3), 244−50 and 3 p following 250..
(37) Yin, J.; Straight, P. D.; McLoughlin, S. M.; Zhou, Z.; Lin, A. J.; Golan, D. E.; Kelleher, N. L.; Kolter, R.; Walsh, C. T. Genetically encoded short peptide tag for versatile protein labeling by Sfp phosphopantetheinyl transferase. *Proc. Natl. Acad. Sci. U. S. A.* **2005**, *102* (44), 15815−20.
(38) Fierz, B.; Poirier, M. G. Biophysics of Chromatin Dynamics. *Annu. Rev. Biophys.* **2019**, *48*, 321−345.

(39) Boyle, E. A.; Andreasson, J. O. L.; Chircus, L. M.; Sternberg, S. H.; Wu, M. J.; Guegler, C. K.; Doudna, J. A.; Greenleaf, W. J. High-throughput biochemical profiling reveals sequence determinants of dCas9 off-target binding and unbinding. *Proc. Natl. Acad. Sci. U. S. A.* **2017**, *114* (21), 5461−5466.
(40) Hinz, J. M.; Laughery, M. F.; Wyrick, J. J. Nucleosomes Selectively Inhibit Cas9 Off-target Activity at a Site Located at the Nucleosome Edge. *J. Biol. Chem.* **2016**, *291* (48), 24851−24856.
(41) Mivelaz, M.; Cao, A. M.; Kubik, S.; Zencir, S.; Hovius, R.; Boichenko, I.; Stachowicz, A. M.; Kurat, C. F.; Shore, D.; Fierz, B. Chromatin Fiber Invasion and Nucleosome Displacement by the Rap1 Transcription Factor. *Mol. Cell* **2020**, *77* (3), 488−500.
(42) North, J. A.; Shimko, J. C.; Javaid, S.; Mooney, A. M.; Shoffner, M. A.; Rose, S. D.; Bundschuh, R.; Fishel, R.; Ottesen, J. J.; Poirier, M. G. Regulation of the nucleosome unwrapping rate controls DNA accessibility. *Nucleic Acids Res.* **2012**, *40* (20), 10215−27.

https://doi.org/10.1021/jacs.1c06195
J. Am. Chem. Soc. 2021, 143, 16313−16319